

Anisotropic crystallization in solution processed chalcogenide thin film by linearly polarized laser

Tingyi Gu^{1,2}, Hyuncheol Jeong³, Kengran Yang^{4,5}, Fan Wu¹, Nan Yao¹,

Rodney D. Priestley^{1,3}, Claire E. White^{4,5} and Craig B. Arnold^{1}*

¹ Princeton Institute for the Science and Technology of Materials, Princeton University, Princeton, New Jersey, 08544

² Electrical and Computer Engineering, University of Delaware, Newark, DE 19716

³ Chemical and Biological Engineering, Princeton University, Princeton, New Jersey 08544

⁴ Civil and Environmental Engineering, Princeton University, Princeton, New Jersey 08544

⁵ Andlinger Center for Energy and the Environment, Princeton University, New Jersey 08544

*Email: cbarnold@princeton.edu

Abstract: The low activation energy associated with amorphous chalcogenide structures offers broad tunability of material properties with laser-based or thermal processing. In this paper, we study near-bandgap laser induced anisotropic crystallization in solution processed arsenic sulfide. The modified electronic bandtail states associated with laser irradiation lead to a distinctive photoluminescence spectrum, compared to thermally annealed amorphous glass. Laser crystallized materials exhibit a periodic subwavelength ripples structure in transmission electron microscopy experiments and show polarization dependent photoluminescence. Analysis of the local atomic

structure of these materials using laboratory-based X-ray pair distribution function analysis indicates that laser irradiation causes a slight rearrangement at the atomic length scale, with a small percentage of S-S homopolar bonds converting to As-S heteropolar bonds. These results highlight fundamental differences between laser and thermal processing in this important class of materials.

Introduction:

Chalcogenide materials have the ability to transform among various states, ranging from random amorphous networks to atomically ordered crystalline states when exposed to modest energy such as that associated with optical or thermal processes [1-4]. These different structures typically exhibit significant optical refractive index contrast, as well as differences in electronic conductivities and other material properties. Among various tuning schemes, laser processing is especially interesting as it enables precise control of the amount of energy delivered into a specific targeted region. Such methods have been explored for tuning integrated photonic devices [5-12] as well as for controlling dichroism or polarization dependent photodarkening phenomena in these materials [13-17]. It has been shown that the precise atomic structure depends on the laser wavelength, duration and intensity of laser irritations [17].

In the case of solution processed chalcogenide materials [4, 11], laser heating from above band-gap illumination has been shown to remove excess solvent related components to densify films and modify the surface chemistry and surface morphology [3]. It has been shown in arsenic sulfide (As_2S_3) that laser heating can induce thermal effects capable of breaking the chalcogenide-solvent bond. Furthermore, laser exposure can affect the structural properties of chalcogenide materials through polarization dependent athermal phenomena [10]. Such process can cause redistribution of atomic clusters or chemical reactions leading to anisotropic properties [13-17].

In this paper we show near-band gap laser irradiation can lead to structural changes unlike those associated with thermal processing. Beginning with a solution processed glass As_2S_3 film, laser processing results in crystallization and corresponding anisotropies in optical properties. Photoluminescence (PL) measurements show well-defined shifts in emission peaks relative to thermally annealed materials while PDF analysis highlights the changes in bonding structure within the films.

As_2S_3 solution is prepared as in prior work by dissolving amorphous As_2S_3 powder in propylamine [11]. This solution is then spin-casted or drop coated on a substrate (TEM grid or silica microscope slide) and thermally processed at different temperatures as specified in the results. Fig. 1a shows the optical image of As_2S_3 drop casted on a TEM grid (carbon coated, copper grid). The TEM grid size is $10\ \mu\text{m}$ by $10\ \mu\text{m}$. A 532nm laser beam and Gaussian beam profile is concentrated in the middle of the film, and the bright circles in Fig. 1a indicate the extent of the laser beam. The dark spot in the center of the laser exposed region shows the laser crystallized area. TEM (Phillips CM200) is performed at 200 keV in bright-field, dark-field, and diffraction conditions. The diffraction pattern of unexposed material shows blurry rings indicating the amorphous nature of the solution processed As_2S_3 (Fig. 1b). In comparison, the diffraction pattern from the center of laser-exposed area shows clear crystalline structure formed under both low ($40\ \mu\text{W}/\mu\text{m}^2$) (Fig. 1c) and high ($160\ \mu\text{W}/\mu\text{m}^2$) (Figure 1d) laser intensity. The measured lattice spacings for the low intensity exposure ($2.636\ \text{\AA}$, $1.512\ \text{\AA}$) correspond to polycrystalline As_4S_4 ($2.636\ \text{\AA}$, $1.513\ \text{\AA}$). Also, the polycrystalline structure shows a preferred orientation indicated with an intensity enhancement in the diffraction as shown in Fig. 1c (marked with a circle). The TEM diffraction pattern of high laser intensity exposure shows distinct periodic spots indicating a single crystal type structures (Fig. 1d). As a small aperture is placed covering only the diffracted beams in the

circled region in Fig. 1c, a dark-field image (Fig. 1e) is formed which shows a Morie pattern of ~10 nm spacing due to the overlap of As₄S₄ nanostructure crystal layers with preferred orientations.

Bruker D8 Advance X-ray diffractometer was used to obtain pair distribution functions (PDFs) of the As₂S₃ system in order to probe its atom-atom correlations. The As₂S₃ solution is dried in a ceramic pestle and resulting powder is loaded into a 2.5-inch long polyimide capillary and sealed using quick-setting transparent epoxy. The material is then uniformly exposed to a 30μW/μm² (low intensity) 532 nm laser for approximately 5 minutes and 120μW/μm² (high intensity) for the same duration. Ag Kα radiation is used, which has a smaller wavelength compared to Cu radiation, and hence provides a broader Q range. A step size of 0.050°, along with a count time per step of 30s, and a 2θ range of 3° to 130° is used. The PDF, $G(r)$, was obtained by taking a sine Fourier transform of the measured total scattering function, $S(Q)$, as shown in equation (1) [18]

$$G(r) = \frac{2}{\pi} \int_{Q_{min}}^{Q_{max}} Q[S(Q) - 1] \sin(Qr) dQ \quad (1)$$

where Q is the momentum transfer given by $Q = 4\pi \sin\theta/\lambda$. Standard data reduction procedures are followed to obtain the PDF using PDFgetX2 [19], with a Q_{max} of ~14.4 Å⁻¹. Prior to calculation of the PDF, the total scattering function is multiplied by a Lorch window function [20] to improve the signal/noise at the expense of real-space resolution.

Fig. 2 displays the X-ray PDF data for the solution processed sample (SP) together with the laser exposed samples at two different intensities. In contrast to the TEM results, where it was clear that laser exposure led to local alterations of the atomic structure (Fig. 1), the PDF data shows minimal changes to the amorphous atomic structure as a result of laser exposure. The first atom-atom correlation in the X-ray PDF at 2.26 Å is assigned to the As-S bond length (denoted as (i) in Fig.

2), while the second correlation at 3.45 Å is attributed to the atom-atom distances of As-As, S-S, and 2nd nearest-neighbor As-S (denoted as (ii) in Fig. 2) [21]. Slight changes to the ratio of the peak intensities at these locations, $G(i) / G(ii)$, as a result of laser exposure, is indicative of rearrangements to the atomic structure. As the intensity of laser exposure increases, the $G(i) / G(ii)$ ratio increases, implying that some of the S-S homopolar bonds are being converted to As-S heteropolar bonds. This observation agrees with the electron diffraction patterns shown in Fig. 1, where upon laser exposure the structure becomes more ordered with a layered anisotropic structure. Hence, the PDF results indicate that exposure to radiation causes the structure to rearrange, although no sign of crystallization is visible in the data using this bulk analysis technique.

Fig. 3a shows Fourier transform infrared spectra (FTIR) of as-spin coated arsenic sulfide without thermal or laser processing, and the same material followed by thermal annealing at 110 °C, 160 °C, and 185 °C, respectively. The broad absorption at 2200-3100 cm^{-1} , indicative of amine molecules, gradually weakens as the material is annealed at higher temperature. The two absorption peaks in the range of 1300 – 1700 cm^{-1} , representing solvent species in the sample, disappear entirely at the annealing temperature of 185°C. The Differential Scanning Calorimetry (DSC) thermograms of solution-processed As_2S_3 powders (red curve in Fig. 3d) exhibits a broad endothermic peak around 135 °C, while the same sample with pre-annealing at 120 °C for 5 hours does not (blue line in Fig. 3d). We expect that the endothermic peak corresponds to the decomposition of sulfur bonds associated with the propylamine dissolution and the removal of H in the form of H_2S as proposed by Chern et al [22]. In addition, we find that temperature around 180 ~ 190°C induced another structural change of the material, as supported by noisy peaks in DSC trace of solution-processed As_2S_3 (Fig. 3d). In comparison to the DSC trace of raw As_2S_3 (black curve in Figure 3d), this temperature matches the expected glass transition (T_g) (Fig. 3e) at

which the material becomes liquid like from the glassy state. T_g in raw material is measured to be near 191.7 °C. The structural changes captured by DSC are consistent with the FTIR measurement results.

The PL spectra were collected by coupling the light scattered from the sample to a Horiba Raman spectrometer through a 100× objective, focusing the probe laser (532 nm) spot to $\sim 1.5 \mu\text{m}^2$. The excitation laser intensity is controlled below $0.4 \mu\text{W}/\mu\text{m}^2$ to minimize nonlinear response and minimize any subsequent modifications to the material. The presence of solvent in As_2S_3 prevents photoluminescence and only samples annealed above 140°C exhibit a strong photoluminescence signal. As the glass restructures with thermal annealing at 160°C and 185°C, the defects levels in solution processed As_2S_3 give rise to a broadband emission spectrum in the visible band, centered at 680nm. In the band diagram inset of Fig. 3b and 3c, the black arrow conceptualizes the As_2S_3 absorption with near bandgap energy, and the grey arrows show photoluminescence from the defects levels. Laser crystallized As_4S_4 has particular defect energy levels compared to thermally processed samples and the PL spectrum shows significant differences (Fig. 3c vs 3b). In particular, the laser irradiated samples show a red shift in the center of the PL spectrum from 680 nm for the thermally processed samples to 750 for the laser processed samples.

Thermal annealing removes solvent species to form isotropic amorphous films, while the polarized laser crystallizes the chalcogenide material (Fig. 1e). The anisotropy of the crystal would be expected to exhibit an excitation polarization dependence in the PL spectrum. After crystallization of the material by high intensity laser (532nm), we probe the modified PL of the crystallized region on the same set-up configuration, but reduce the laser power to monitor the PL spectrum. Figure 4a shows the PL spectrum from laser crystallized materials under different excitation polarizations

of 0° , 45° , 90° , 135° and 180° . The polarization degree is relative to the one of crystallization laser. We see that the maximum emission intensity occurs for 90° showing a 50% enhancement of photoluminescence relative to the parallel polarization (0°) further confirming the preferred anisotropy in the polycrystalline structure shown in Fig. 1c.

We studied the localized atomic structure change in solution processed arsenic sulfide by near bandgap laser exposure. Fundamental differences between thermal and laser-based processing are observed by thermal, optical, X-ray and electron microscopy characterization corresponding to differences in the structural properties of the material. These locally crystallized anisotropic chalcogenide materials could be incorporated for designing new components in integrated photonic devices.

AUTHOR INFORMATION

Correspondent Author

*E-mail: cbarnold@princeton.edu

Notes

The authors declare no competing financial interest.

ACKNOWLEDGMENT

The authors thank intriguing discussions with Prof. Yueh-Lin Loo of Princeton University, and facility at Imaging and Analysis Center at Princeton University. This work was supported by NSF through the MIRTHE Center (Grant No. EEC-0540832) and MRSEC Center (Grant No. DMR-1420541).

References:

- [1] V. Weidenhof, I. Friedrich, S. Ziegler, M. Wuttig, Laser induced crystallization of amorphous Ge₂Sb₂Te₅ films, *Journal of Applied Physics* **89**, 3168-76 (2001).
- [2] H. F. Hamann, M. O'Boyle, Y. C. Martin, M. Rooks, H. K. Wickramasinghe, Ultra-high-density phase-change storage and memory, *Nature Materials* **5**, 383-7 (2006).
- [3] D. Savytskii, B. Knorr, V. Dierolf, H. Jain, Challenges of CW laser-induced crystallization in a chalcogenide glass, *Optical Materials Express* **3**, 1026-38 (2013).
- [4] S. Song, J. Dua and C. B. Arnold, Influence of annealing conditions on the optical and structural properties of spin-coated As₂S₃ chalcogenide glass thin films, *Optics Express* **18**, 5472-80 (2010).
- [5] C. Markos, Photo-induced changes in a hybrid amorphous chalcogenide/silica photonic crystal fiber, *Applied Physics Letters* **104**, 011114 (2014).
- [6] D. Sridharan, E. Waks, G. Solomon, J. T. Fourkas, Reversible tuning of photonic crystal cavities using photochromic thin films, *Applied Physics Letters* **96**, 153303 (2010).
- [7] A. Faraon, D. Englund, D. Bulla, B. Luther-Davies, B. J. Eggleton, N. Stoltz, P. Petroff, and J. Vučković, Local tuning of photonic crystal cavities using chalcogenide glasses, *Applied Physics Letters* **92**, 043123 (2008).
- [8] A. Canciamilla, F. Morichetti, S. Grillanda, P. Velha, M. Sorel, V. Singh, A. Agarwal, L. C. Kimerling, A. Melloni, Photo-induced trimming of chalcogenide-assisted silicon waveguides. *Optics Express* **20**, 15807-17 (2012).

- [9] A. Canciamilla, S. Grillanda, F. Morichetti, C. Ferrari, J. Hu, J. D. Musgraves, K. Richardson, A. Agarwal, L. C. Kimerling, A. Melloni, Photo-induced trimming of coupled ring-resonator filters and delay lines in As_2S_3 chalcogenide glass, *Optics Letters* **36**, 4002-4 (2011).
- [10] C. Lu, D. Recht, and C. B. Arnold, Generalized model for photoinduced surface structure in amorphous thin films, *Physics Review Letters* **111**, 105503 (2013).
- [11] Y. Zha, M. Waldmann, and C. B. Arnold, A review on solution processing of chalcogenide glasses for optical components, *Optical Material Express* **3**, 1259-1272 (2013).
- [12] C. D' Amico, C. Caillaud, P. K. Velpula, M. K Bhuyan, M. Somayaji, J.-P. Columbier, J. Troles, L. Calvez, V. Nazabal, A. Boukenter, and R. Stoian, Ultrafast laser-induced refractive index changes in $\text{Ge}_{15}\text{As}_{15}\text{S}_{70}$ chalcogenide glass, *Optical Material Express* **6**, 1914-1928 (2016)
- [13] G. Chen, H. Jain, M. Vlcek, S. Khalid, J. Li, D. A. Drabold, S. R. Elliott, Observation of light polarization-dependent structural changes in chalcogenide glasses, *Applied Physics Letters* **82**, 706-8 (2013).
- [14] V. Lyubin, M. Klebanov, M. Mitkova, T. Petkova, Polarization-dependent, laser-induced anisotropic photocrystallization of some amorphous chalcogenide films, *Applied Physics Letters* **71**, 2118-20 (1997).
- [15] V. M. Lyubin, M. L. Klebanov, Laser-induced anisotropic absorption, reflection, and scattering of light in chalcogenide glassy semiconductors, *Semiconductors* **32**, 817-23 (1998).

- [16] K. Richardson, T. Cardinal, M. Richardson, A. Schulte, S. Seal, in Engineering Glassy chalcogenide materials for integrated optics applications, ed. By A. V. Koloboc, Photoinduced metastability in amorphous semiconductors (Wiley-VCH, Weinheim 2003)
- [17] K. Antoine, H. Jain, M. Vlcek, S. D. Senanayake, D. A. Drabold, Chemical origin of polarization-dependent photoinduced changes in an $\text{As}_{36}\text{Se}_{64}$ glass film via in situ synchrotron x-ray photoelectron spectroscopy, *Physical Review B* **79**, 054204 (2009).
- [18] E. Takeshi and S. J. L. Billinge, *Underneath the Bragg Peaks: Structural Analysis of Complex Materials*, Elsevier (2003).
- [19] X. Qiu, J. W. Thompson and S. J. L. Billinge, PDFgetX2: a GUI-driven program to obtain the pair distribution function from X-ray powder diffraction data, *Journal of Applied Crystallography* **37**, 678 (2004).
- [20] E. Lorch, Neutron diffraction by germania, silica and radiation-damaged silica glasses, *Journal of Physics C: Solid State Physics* **2**, 229–237 (2002).
- [21] D. J. E. Mullen, W. Nowacki, Refinement of crystal structures of realgar, AsS and orpiment, As_2S_3 , *Zeitschrift für Kristallographie* **136**, 48-65 (1972).
- [22] G. C. Chern, I. Lauks and A. R. McGhie, Spin Coated Amorphous Chalcogenide Films: Thermal Properties, *Journal of Applied Physics* **54**, 4596–4601 (1983).

Figures:

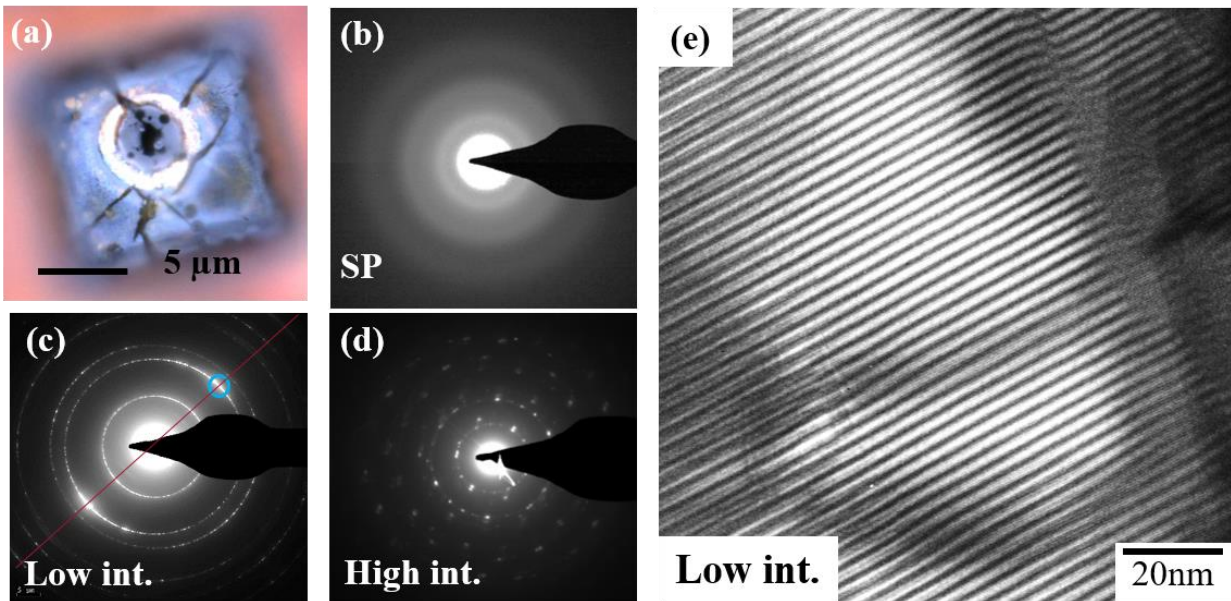


Figure 1. Laser Gaussian beam induced pattern on chalcogenide thin film. (a) Optical image of solution processed As_2S_3 film drop-casted on TEM grid, observed under 100x microscope after laser exposure of 10 second, with average power of $160\mu\text{W}/\mu\text{m}^2$. Scale bar: $5\mu\text{m}$. (b) Electron diffraction pattern for the unexposed region and (c) Crystallized region near the center of the beam ($40\mu\text{W}/\mu\text{m}^2$). The red line shows the preferred nanocrystal orientation. (d) The crystallized region after laser exposure with $160\mu\text{W}/\mu\text{m}^2$. (e) A corresponding dark-field image showing the real-space structure as in (c), through the aperture in the blue circle.

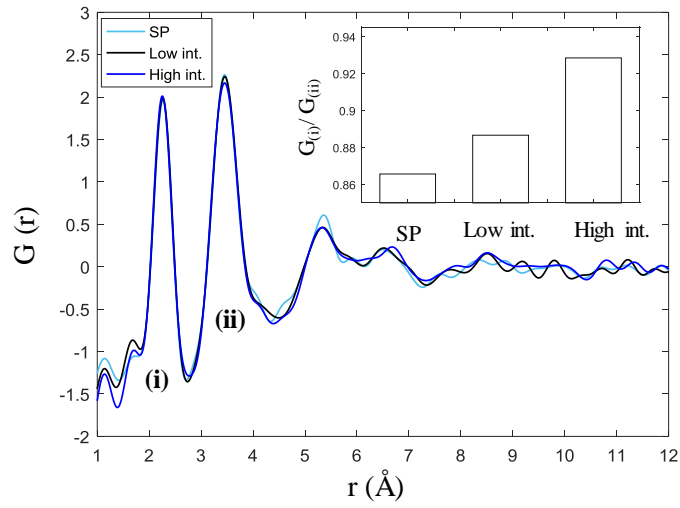


Figure 2. Laboratory X-ray PDF data for solution processed sample (SP), after low intensity laser exposure (532nm, $30\mu\text{W}/\mu\text{m}^2$) and high intensity laser exposure (532nm, $120\mu\text{W}/\mu\text{m}^2$), Inset: The peak intensity ratio of the first nearest neighbor correlation intensity (i) to the second (ii).

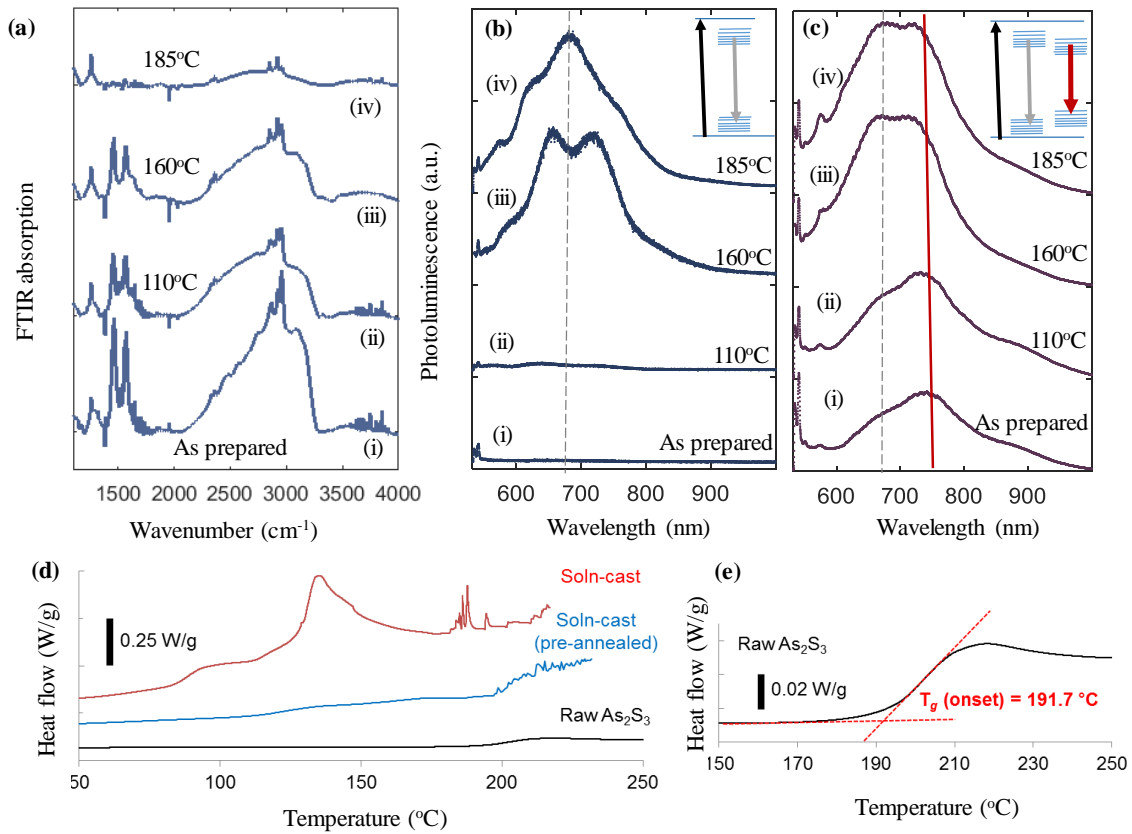


Figure 3. Photoluminescence of laser and thermal induced defects. (a) FTIR measurement of spin coated sample before (i) and after annealing in nitrogen environment at (ii) 110°C (iii) 160°C and (iv) 185°C for 5 hours. Note, curves all have same scale but are shifted on the y-axis for clarity. (b) Photoluminescence of corresponding samples shown in (a). Grey dashed line marks the center wavelength of the thermal induced defects state. Inset: band diagram and absorption (black arrow) and emission (grey arrow) from the thermal induced defects. Spectra are individually normalized and shifted for clarity. (c) Photoluminescence of spin coated sample after $40\mu\text{W}/\mu\text{m}^2$ laser exposure for 10s. The grey dashed line and red solid line mark the center wavelength of amorphous thermally annealed sample and laser crystallized structure, respectively. Inset: absorption (black arrow), emission from thermal induced (grey arrow) and laser induced (red) defects. (d) Differential scanning calorimetry (DSC) thermograms of raw (black), solution processed (blue)

and pre-annealed (120°C for 5 hours in vacuum of solution processed sample) arsenic sulfide. The heating rate is 10°C/min. (e) Magnified DSC measurement showing the glass transition of raw arsenic sulfide.

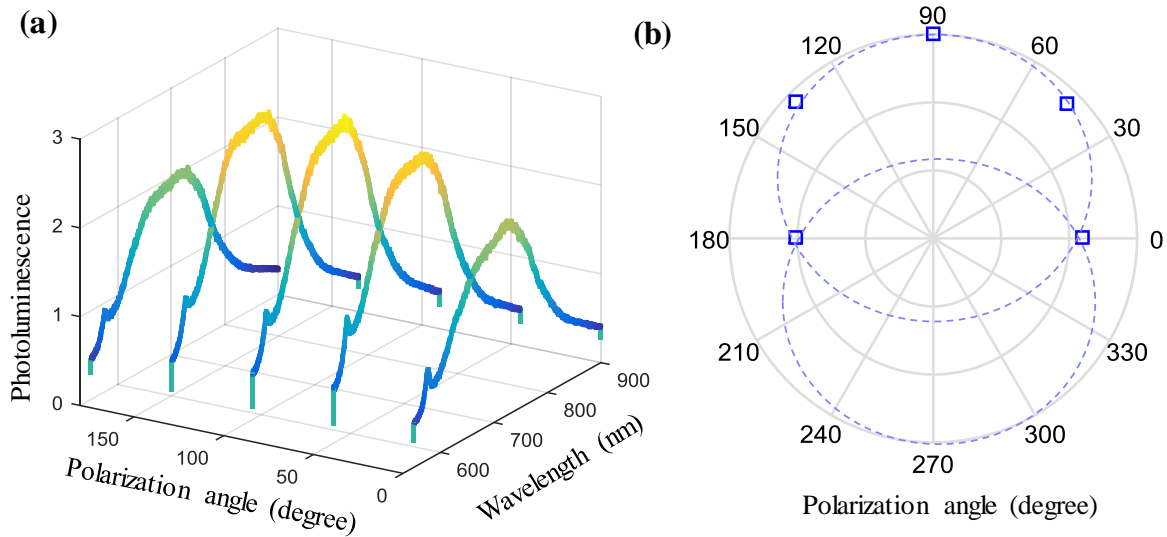


Figure 4. Photoluminescence spectra of the laser crystallized chalcogenide. (a) Photoluminescence spectra, (b) intensity versus relative polarization angle to the crystallization laser. The blue squares are experimental data and the dashed circles are fitted circles.